

This discussion paper is/has been under review for the journal Biogeosciences (BG).  
Please refer to the corresponding final paper in BG if available.

# Impact of an extremely large magnitude volcanic eruption on the global climate and carbon cycle estimated from ensemble Earth System Model simulations

J. Segschneider<sup>1</sup>, A. Beitsch<sup>1,\*</sup>, C. Timmreck<sup>1</sup>, V. Brovkin<sup>1</sup>, T. Ilyina<sup>1</sup>,  
J. Jungclaus<sup>1</sup>, S. J. Lorenz<sup>1</sup>, K. D. Six<sup>1</sup>, and D. Zanchettin<sup>1</sup>

<sup>1</sup>Max-Planck-Institut für Meteorologie, Bundesstr. 53, 20146 Hamburg, Germany  
\*now at: Institute for Oceanography, KlimaCampus, University of Hamburg, Germany

Received: 25 May 2012 – Accepted: 1 June 2012 – Published: 18 July 2012

Correspondence to: J. Segschneider (joachim.segshneider@zmaw.de)

Published by Copernicus Publications on behalf of the European Geosciences Union.

**BGD**

9, 8693–8732, 2012

**Impact of  
supervolcanic  
eruptions on the  
Earth System**

J. Segschneider et al.

Title Page

Abstract

Introduction

Conclusions

References

Tables

Figures

⏪

⏩

◀

▶

Back

Close

Full Screen / Esc

Printer-friendly Version

Interactive Discussion

## Abstract

The response of the global climate-carbon cycle system to an extremely large Northern Hemisphere mid latitude volcanic eruption is investigated using ensemble integrations with the comprehensive Earth System Model MPI-ESM. The model includes dynamical compartments of the atmosphere and ocean and interactive modules of the terrestrial biosphere as well as ocean biogeochemistry. The MPI-ESM was forced with anomalies of aerosol optical depth and effective radius of aerosol particles corresponding to a super eruption of the Yellowstone volcanic system. The model experiment consists of an ensemble of fifteen model integrations that are started at different pre-ENSO states of a control experiment and run for 200 yr after the volcanic eruption. The climate response to the volcanic eruption is a maximum global monthly mean surface air temperature cooling of 3.8 K for the ensemble mean and from 3.3 K to 4.3 K for individual ensemble members. Atmospheric  $p\text{CO}_2$  decreases by a maximum of 5 ppm for the ensemble mean and by 3 ppm to 7 ppm for individual ensemble members approximately 6 yr after the eruption. The atmospheric carbon content only very slowly returns to near pre-eruption level at year 200 after the eruption. The ocean takes up carbon shortly after the eruption in response to the cooling, changed wind fields, and ice cover. This physics driven uptake is weakly counteracted by a reduction of the biological export production mainly in the tropical Pacific. The land vegetation pool shows a distinct loss of carbon in the initial years after the eruption which has not been present in simulations of smaller scale eruptions. The gain of the soil carbon pool determines the amplitude of the  $\text{CO}_2$  perturbation and the long term behaviour of the overall system: an initial gain caused by reduced soil respiration is followed by a rather slow return towards pre-eruption levels. During this phase, the ocean compensates partly for the reduced atmospheric carbon content in response to the land's gain. In summary, we find that the volcanic eruption has long lasting effects on the carbon cycle: after 200 yr, the ocean and the land carbon pools are still different from the pre-eruption state, and

## Impact of supervolcanic eruptions on the Earth System

J. Segschneider et al.

Title Page

Abstract

Introduction

Conclusions

References

Tables

Figures



Back

Close

Full Screen / Esc

Printer-friendly Version

Interactive Discussion



the land carbon pools (vegetation and soil) show some long lasting local anomalies that are only partly visible in the global signal.

## 1 Introduction

Volcanic super eruptions are very rare events of exceptional magnitude (Self and Blake, 2008) that have a strong impact on the Earth System. While this is relatively well known for the climate system, less research has been carried out to estimate the impact on the carbon cycle of both land and ocean and the resulting perturbations of the atmospheric CO<sub>2</sub> content. Here we investigate the short and long term (up to 200 yr) impact of a super volcanic eruption on the Earth System including the global carbon cycle.

Well known volcanic super eruptions are the 74 kyr B.P. Toba and the three extremely large eruptions at the geographical site of Yellowstone (44° N, 110° W). Due to their large radiative forcing super volcanic eruptions affect the climate system significantly (Jones et al., 2005; Self, 2006; Robock et al., 2009; Timmreck et al., 2010). It has even been speculated for the 74 kyr B.P. Toba eruption that the resulting climate perturbation brought modern human society close to the brink of extinction (Ambrose, 1998; Williams, 2009) due to the induced temperature decrease. However, care has to be taken when relating mass of ejected SO<sub>2</sub> to climate perturbation. Timmreck et al. (2010, 2012) show that the volcanic maximum cooling does not increase linearly with the amount of total stratospheric sulphur injection, because of multiple limiting effects, including those based on radiation transmission (Beer–Bouguer–Lambert law) and the increase in particle size (Timmreck et al., 2012).

Large climatic perturbations have a potential to perturb the global carbon cycle. The latter is sensitive to changes in solar radiation, temperature, sea ice cover, and atmospheric and oceanic circulation. Model estimates of the impact of volcanic eruptions on climate and carbon cycle using comprehensive Earth System Models (ESMs) that include an interactive carbon cycle are a relatively recent achievement. The employed models describe not only the dynamical components of the climate system, but also the

**BGD**

9, 8693–8732, 2012

## Impact of supervolcanic eruptions on the Earth System

J. Segschneider et al.

Title Page

Abstract

Introduction

Conclusions

References

Tables

Figures

⏪

⏩

◀

▶

Back

Close

Full Screen / Esc

Printer-friendly Version

Interactive Discussion



respective carbon cycle compartments, namely the land vegetation and soil as well as the carbonate chemistry and the ecosystem of the ocean. Such models can be forced with anomalies of aerosol optical depth (AOD) and effective radius of aerosol particles ( $R_{\text{eff}}$ ) corresponding to the sulfate aerosol cloud that develops after a volcanic eruption.

5 An early ESM study has been performed with the Hadley Centre Climate Model HadCM3 for the 1991 Mt. Pinatubo eruption (Jones and Cox, 2001). The authors show that the volcano induced cooling (about 0.4 K for the global mean surface temperature in their model, which is comparable to observed estimates, Thompson et al., 2009) is likely to have a measurable and significant effect on the carbon cycle. As  
10 the main mechanism, they identify globally reduced soil and plant respiration amplified by increased terrestrial primary productivity due to increased rainfall in the tropical rainforests of the Amazon and Central Africa. For the ocean, the authors do not find significant variations in the uptake or release of carbon in response to the Mt. Pinatubo eruption.

15 Brovkin et al. (2010) analyse the carbon cycle response of the Max Planck Institute for Meteorology Earth System Model (MPI-ESM, Jungclaus et al., 2010) to the 1258 AD volcanic eruption. This is the largest known eruption in the period 800–2000 AD, but the exact location is unknown. They simulate a global mean cooling of almost 1 K that lasts for a few years. In response to the cooling, the atmospheric  $p\text{CO}_2$  decreases by  
20 about 2 ppm. In contrast to the study of Jones and Cox (2001) also the ocean carbon pool responds to the volcanic forcing. It initially takes up about 1 GtC, but then quickly loses carbon to the atmosphere, compensating the carbon gain by the land biosphere.

25 Tjiputra and Ottera (2011) investigate the potential of volcanic eruptions to delay global warming and to alter the global carbon cycle in a scenario of rising atmospheric  $\text{CO}_2$  with the Bergen Earth System Model (BCM-C). In particular, they simulate either a Pinatubo like eruption (Volcanic Explosivity Index VEI 6) every 5 yr or a Tambora like (VEI 7) eruption every 25 yr for the period 2000 to 2100 in a model experiment where  $\text{CO}_2$  emissions follow the IPCC-A2 scenario. They demonstrate that the smaller but more frequent eruptions have a larger impact on the carbon cycle than the less

**BGD**

9, 8693–8732, 2012

## Impact of supervolcanic eruptions on the Earth System

J. Segschneider et al.

Title Page

Abstract

Introduction

Conclusions

References

Tables

Figures

⏪

⏩

◀

▶

Back

Close

Full Screen / Esc

Printer-friendly Version

Interactive Discussion

frequent larger eruptions. At the end of the integration in 2100, the atmospheric  $p\text{CO}_2$  is 46 ppmv lower than in a control experiment without volcanic forcing.

Frölicher et al. (2011) investigate low-latitude volcanic eruptions of different strength including super volcanic eruptions with the NCAR CSM1.4-carbon model for a 20 yr period. Their forcing in terms of AOD at  $55\ \mu\text{m}$  ( $\text{AOD}_{55\ \mu\text{m}}$ ) perturbation varies from 1 to 100 times that of the 1991 Mt. Pinatubo eruption. The authors find a similar response of the climate-carbon cycle system to the AOD perturbation as Brovkin et al. (2010). Moreover, anomalies in the subsurface ocean prevail for 20 yr (their model integration length). 20 yr, however, is too short to investigate the long term impact and the duration of the perturbation of the carbon cycle. Moreover, Frölicher et al. (2011) perform only one realisation for each forcing strength which makes it impossible to estimate the impact of climatic initial conditions at the time of eruption and relate this uncertainty to the volcanic signal.

In a recent discussion paper Rothenberg et al. (2012) describe the response of the Community Climate Model Version 3 (CCSM3) to tropical volcanic eruptions as represented by the time-varying volcanic forcing from Ammann et al. (2003) in the period 1870 to 2000 and the 1991 Pinatubo eruption in particular. They find that while their precipitation anomalies are comparable to observations, the carbon cycle anomalies are smaller than observed and also smaller than modelled by Jones and Cox (2001). As they also find that the precipitation anomalies in Jones and Cox (2001) are too strong, they suspect that the correct carbon cycle anomalies in that paper may stem from incorrect climate anomalies. Moreover, Nemani et al. (2003) show that plant growth in the Amazon region is limited by radiation, not precipitation. From this, a decrease in NPP in the Amazon region in response to decreased radiation seems a more likely response to volcanic eruptions.

In this study we advance beyond previous work by investigating a Yellowstone type Northern Hemisphere severe eruption as simulated by an atmospheric circulation and chemistry model in an ensemble simulation including the long term response. We chose the geographical site of Yellowstone, because it is one of the most likely sites

**BGD**

9, 8693–8732, 2012

## Impact of supervolcanic eruptions on the Earth System

J. Segschneider et al.

Title Page

Abstract

Introduction

Conclusions

References

Tables

Figures

⏪

⏩

◀

▶

Back

Close

Full Screen / Esc

Printer-friendly Version

Interactive Discussion





GR30L40 (nominally 3°, with a higher resolution in the North Atlantic, and 40 layers, with higher vertical resolution in the upper part of the water column). The MPI-ESM response of the physical atmosphere-ocean model system to large volcanic eruptions is described in Zanchettin et al. (2011). As the MPI-ESM components are described in detail elsewhere, we only provide a short description of the model's land and ocean carbon cycle, mainly to allow a better understanding of the processes that will respond to the volcanic eruption.

The oceanic carbon cycle model HAMOCC works on the same grid as the physical ocean model. It simulates the full carbonate chemistry (Maier-Reimer, 1993) and a simplified, so-called NPZD type, biological system (Six and Maier-Reimer, 1996). The latter consists of the nutrients (N) phosphate, nitrate, silicate, and iron, and phytoplankton (P), implicitly divided between coccolithophores and diatoms depending on the availability of silicate. Grazing of phytoplankton by zooplankton (Z) and the sinking of detritus (D) are also part of the model. With regard to our analysis it is important to keep in mind that (i) the solubility of CO<sub>2</sub> in seawater depends mainly on the temperature, and (ii) the productivity of the marine ecosystem on availability of nutrients, short wave radiation, and temperature. Moreover, it is the sinking of detritus out of the surface ocean that determines the strength of the biological pump, not the biological production as such. Carbon fluxes between the ocean and the atmosphere are computed depending on the difference in partial pressure between the two components, and the so-called piston velocity, which depends mainly on wind speed. Additionally, sea ice will inhibit any flux for entirely ice-covered grid cells.

The land surface component JSBACH operates with the same spatial and temporal resolution as the atmospheric model ECHAM (here T31). The vegetation is represented by several plant functional types (trees, grasses, shrubs, and pastures), and gross primary productivity depends on shortwave radiation, temperature, CO<sub>2</sub> concentration, and moisture availability. The soil carbon is described by one slow and one fast reacting pool. Accumulation of carbon in the soil pool due to litter fall is an instantaneous

**BGD**

9, 8693–8732, 2012

## Impact of supervolcanic eruptions on the Earth System

J. Segschneider et al.

Title Page

Abstract

Introduction

Conclusions

References

Tables

Figures



Back

Close

Full Screen / Esc

Printer-friendly Version

Interactive Discussion



process, while the mineralization rate of soil organic carbon is a function of temperature ( $Q_{10} = 1.8$ ) and soil moisture.

## 2.2 Potential effects of volcanic eruptions on climate and the global carbon cycle

5 In the MPI-ESM, the volcanic eruption as represented by AOD and  $R_{\text{eff}}$  perturbations has several effects on the climate and the carbon cycle (Fig. 1). In the atmosphere, the main effect is a reduction in short wave radiation (SWR) due to increased aerosol loading with the associated cooling of the troposphere and thus also the land and ocean surface. Cooling of the ocean will increase the solubility of  $\text{CO}_2$  in sea water,  
10 driving an anomalous carbon flux from the atmosphere to the ocean. A reduction of the SWR and the cooling, on the other hand, will have a negative impact on marine biological production rates, thereby weakening the biological pump. This would drive an anomalous carbon flux from the ocean to the atmosphere. Ash input from the volcano could potentially fertilize the ocean (not included in the main experiment of this study).

15 For the land biosphere, a cooling will reduce soil respiration, driving a flux from the atmosphere to the soil. The land vegetation carbon pool, as for the ocean, will decrease in response to reduced SWR and temperature, potentially driving a flux from the land into the atmosphere. Changes in precipitation and wind patterns also have potential for changing carbon fluxes, but these are less straightforward to estimate even with regard  
20 to their sign.

## 2.3 Experiment design

We follow a two step approach as in Timmreck et al. (2010). First, the formation and temporal development of the volcanic aerosol and the corresponding radiative forcing from an initial injection of  $\text{SO}_2$  are simulated with the global aerosol atmospheric model  
25 MAECHAM5/HAM (Niemeier et al., 2009) in T42L39 resolution. Important initialization parameters for a volcanic super eruption, namely the stratospheric sulphur emission,

## Impact of supervolcanic eruptions on the Earth System

J. Segsneider et al.

Title Page

Abstract

Introduction

Conclusions

References

Tables

Figures

⏪

⏩

◀

▶

Back

Close

Full Screen / Esc

Printer-friendly Version

Interactive Discussion



the eruption height, and the duration of the eruption are highly uncertain even though there exist some estimates about the ejected mass in terms of dry rock equivalent.

We therefore investigate a generic NH mid-latitude super eruption with a reasonable/likely parameter set up. We chose the same parameters as for the chemistry climate model study MAECHAM4/CHEM (Timmreck and Graf, 2006) and for the MPI-ESM study of the tropical Young Toba Tuff eruption (Timmreck et al., 2010, 2012). The magnitude of the Younger Toba Tuff (YTT) and Yellowstone eruptions in terms of SO<sub>2</sub> injection into the atmosphere is about 100 times that of the 1991 Mt. Pinatubo eruption (17 Mt SO<sub>2</sub>, Read et al., 1993). We thus assume an initial sulfur injection of 1700 Mt SO<sub>2</sub>. This SO<sub>2</sub> was released in the MAECHAM5/HAM model over 10 days in June at the grid box corresponding to the geographical coordinates of Yellowstone (44° N, 110° W) and the pressure level of 30 hPa (ca. 25 km). The volcanic forcing is then calculated online in terms of AOD and  $R_{\text{eff}}$  for every grid point of the model and stored as monthly and zonal mean for a period of 4.5 yr.

Because the aerosol optical depth (AOD) perturbation scales quite differently to eruption strength than the SO<sub>2</sub> injection, the resulting AOD perturbation is much less than the assumption of 100 times Pinatubo. Timmreck et al. (2010) compute a scaling factor of only about 30 instead of 100 for the maximum global mean AOD perturbation. This reduction is mainly due to the formation of larger aerosols than for smaller scale eruptions. These aerosols fall out of the atmosphere more rapidly than smaller ones.

In a second step, the MPI-ESM is forced with the obtained AOD and  $R_{\text{eff}}$  anomalies as 48 zonal means. To provide an estimate of the variability of the model system response, a 15 member ensemble is created by starting the model at different ENSO states of a 2000 yr control integration. We chose to select the ENSO state of the model to generate our ensemble because, on interannual time scales, it has a large impact on the global climate (Penland et al., 2010) as well as on the carbon cycle (Winguth et al., 1994). The different states used correspond to strong El Niño, moderate El Niño, neutral, moderate La Niña, and strong La Niña events. The control run was then analyzed with regard to the ENSO state, and for each of the five classes three simulations are

**BGD**

9, 8693–8732, 2012

## Impact of supervolcanic eruptions on the Earth System

J. Segschneider et al.

Title Page

Abstract

Introduction

Conclusions

References

Tables

Figures

⏪

⏩

◀

▶

Back

Close

Full Screen / Esc

Printer-friendly Version

Interactive Discussion

initialized at different times. The AOD perturbations are applied starting from month 6 of each model simulation. Each of the resulting 15 members is run for 200 yr, resulting in a total of 3000 model years for the entire experiment. The long integration times are needed to cover the tail of the return to pre-eruption levels in particular for the carbon cycle components. We do not perform simulations with different eruption strength here, but will include some features of the model's response to the 1258 AD eruption described in Brovkin et al. (2010) in the discussion of model results.

We diagnose the model output with regard to climate parameters and the carbon pools over the entire 200 yr by computing anomalies with respect to the respective years of the unperturbed control run rather than to compare them with the control run mean. Thus we exclude anomalies arising from the internal long term variability of the control run when computing anomalies. The method also assures that anomalies start with zero at the onset of the volcanic eruption. We will show time series of the anomalies for the ensemble mean and individual members, and maps of monthly mean ensemble mean anomalies at selected times. The times were selected by subjective analysis of 120 monthly mean anomaly maps for the first 10 yr of the experiment.

### 3 Results

#### 3.1 Climate response

First the climatic response of the model is described. Information about significance of results is given by grey shading in time series figures ( $\pm 2\sigma$  level including the annual cycle) and stippling in maps where anomalies exceed the local  $2\sigma$  level of the control experiment for the respective month. The temporal evolution of the globally averaged surface air temperature (SAT) is shown in Fig. 2 for (a) the entire 200 yr period of each experiment and (b) for the initial 20 yr. We will use Fig. 2a to describe the temporal evolution of the SAT anomalies, and Fig. 2b to better describe the magnitude of the perturbations. SAT in all experiments drops rapidly to a minimum value within the first

**BGD**

9, 8693–8732, 2012

## Impact of supervolcanic eruptions on the Earth System

J. Segschneider et al.

Title Page

Abstract

Introduction

Conclusions

References

Tables

Figures

⏪

⏩

◀

▶

Back

Close

Full Screen / Esc

Printer-friendly Version

Interactive Discussion





pronounced temperature perturbation dichotomy with stronger cooling over the Northern Hemisphere, and in particular in the Southern Ocean the cooling is only between 0 K and 2 K and rarely statistically significant.

The zonal wind stress  $\tau_x$  (Fig. 5a–d) develops strong anomalies 12 months after the volcanic eruption: a negative anomaly spans the entire globe between 30–50° S, and a band of positive anomalies is centred around 60° S. This indicates a southward shift of the Southern Hemisphere westerlies, but the anomalies are not significant with regard to the internal variability of the control experiment. This anomalous pattern persists for about 2 yr and then slowly becomes weaker. Even though the anomalies are not statistically significant, the shift has the potential to perturb the marine carbon cycle through upwelling of nutrients and carbon rich deeper waters as well as changing the piston velocity of gas exchange between ocean and atmosphere.

The supply of surface waters with nutrients as well as carbon rich subsurface waters depends on the subsurface concentration and the upwelling velocity. In Fig. 6 we show maps of Ekman Pumping anomalies. The strongest signal comes from the equatorial belt in all ocean basins, but it is statistically significant at the  $2\sigma$  level only in month 24 (Fig. 6c). The Western Pacific shows persistently positive anomalies, while the anomalies change sign in the Eastern Pacific and the Atlantic and Indian Ocean. North and south of the equator anomalies of opposite sign prevail. In the southern mid-latitudes weak negative anomalies can be seen, and a tendency for slightly positive values in higher southern latitudes.

Anomalies in sea ice cover also have a potential to effect carbon fluxes: any increase of sea ice cover as a result of the cooling will strongly inhibit carbon fluxes between ocean and atmosphere and suppress oceanic biological production. To estimate if this is important, we show maps of sea ice cover anomalies (Fig. 7). Sea ice cover fraction increases in the Northern Hemisphere from month 18 (Fig. 7a). At the time of maximum ice extension in the respective hemisphere anomalies are largest in months 21 and 27 (Fig. 7b,c). Interestingly, larger than normal ice cover prevails until month 72 in the Northern Hemisphere (Fig. 7d). In the Southern Hemisphere sea ice cover first

**BGD**

9, 8693–8732, 2012

## Impact of supervolcanic eruptions on the Earth System

J. Segschneider et al.

Title Page

Abstract

Introduction

Conclusions

References

Tables

Figures

⏪

⏩

◀

▶

Back

Close

Full Screen / Esc

Printer-friendly Version

Interactive Discussion

increases briefly, but then decreases from end of year 3. The involved areas are, however, not very large and therefore unlikely to play an important role in driving carbon cycle anomalies.

## 3.2 Carbon cycle response

### 3.2.1 Globally integrated response

Next we investigate the response of the different compartments of the carbon cycle to the climate perturbation. Figure 8 shows timeseries of globally summed-up anomalies in GtC for the atmosphere, ocean, and land. For the land compartment, there is a further separation into soil and vegetation.

The dominating signal in the atmosphere is a decrease of carbon content over the first 6 yr of around 10 GtC for the ensemble mean and up to 14 GtC for individual members). This corresponds to a maximum decrease of atmospheric  $p\text{CO}_2$  by about 7 ppm (5 ppm for the ensemble mean, see also Fig. 9). The decline is followed by a slow but steady return towards pre-eruption levels. This takes much longer than for SAT: the ensemble mean atmospheric carbon pool content is back in the  $2\text{-}\sigma$  range of the control experiment after about 50 yr. A small perturbation even remains until the end of the integration at year 200 (about  $-1$  GtC).

The ocean compartment shows an initial gain of about 4–6 GtC having its maximum in year 4. This is followed by a rapid loss of carbon to the atmosphere that results in values of about 4–8 GtC below pre-eruption level around 50 yr after the volcanic eruption. After this, a very slow recovery is simulated, so slow that at the end of the integration the ensemble mean oceanic carbon content is around 3 GtC less than before the eruption.

The land compartment shows an initial decrease of up to 8 GtC from year 2–4, mainly caused by a drop in the vegetation pool. This drop is accompanied by a smaller decrease in the soil pool in year 3–4, likely due to reduced litter input. After that, a rapid increase to up to 14 GtC occurs, driven by the soil pool, followed by a slow return

**BGD**

9, 8693–8732, 2012

## Impact of supervolcanic eruptions on the Earth System

J. Segsneider et al.

Title Page

Abstract

Introduction

Conclusions

References

Tables

Figures

⏪

⏩

◀

▶

Back

Close

Full Screen / Esc

Printer-friendly Version

Interactive Discussion



towards pre-eruption values in around year 160. This longer term behaviour is also determined by the soil pool. The vegetation pool mainly shows weak fluctuations within the standard variation of the control run after year 4. At the end of the integration in year 200, the land carbon pool contains slightly more carbon (4 GtC for the ensemble mean) than before the eruption.

The impact of the initial state of the model at the time of eruption for the carbon pools is similarly unclear as for SAT. For example, when looking at the atmospheric pool in Fig. 8b, the El Niño-started runs show a more immediate decrease than the La Niña started runs in the first 2 yr, but the latter then continue to drop whereas the El Niño started runs show a temporal increase in carbon content. At the time of maximum anomaly, more La Niña started runs show larger than ensemble mean anomalies, but this is also the case for an El Niño started run. Likewise, one La Niña started run shows weaker than average response to the volcanic eruption. For the soil compartment, there is a tendency for the El Niño started runs to develop an initial positive anomaly up to year 2, but in the total land response this becomes less clear.

### 3.2.2 Oceanic carbon cycle response

In this section we further focus on the marine carbon cycle, beginning with a description of the temporal and spatial evolution of the sea-to-air carbon fluxes. Figure 5e–h shows selected maps of monthly mean air–sea carbon flux anomalies. Positive values indicate an anomalous flux from the ocean to the atmosphere. The anomaly of CO<sub>2</sub> flux between ocean and atmosphere (Fig. 5e–h) shows, most pronounced in the Southern Ocean in southern winter, a tendency for negative anomalies (flux into the ocean) in areas of positive  $\tau_x$ -anomalies and positive anomalies (flux into the atmosphere) in areas of negative  $\tau_x$ -anomalies (Fig. 5b, f). These anomalies, however, are not statistically significant as internal variability is notoriously high in the Southern Ocean. In the low to mid latitudes, however, the simulated CO<sub>2</sub>-flux anomalies are statistically significant even though they are much smaller. As the CO<sub>2</sub>-flux is driven not only by

**BGD**

9, 8693–8732, 2012

## Impact of supervolcanic eruptions on the Earth System

J. Segschneider et al.

Title Page

Abstract

Introduction

Conclusions

References

Tables

Figures

⏪

⏩

◀

▶

Back

Close

Full Screen / Esc

Printer-friendly Version

Interactive Discussion

changing wind fields but also by changes in temperature and export production there is, however, no one-to-one relationship in particular in southern summer (Fig. 5c, g).

In the northern winter of year 2/3, anomalous fluxes into the atmosphere show up in northern high latitudes. These are only partly related to  $\tau_x$  (Fig. 5c, g). An explanation could be the increased sea ice cover (Fig. 7c) in response to the temperature drop. In the Southern Ocean the timing of maximum anomalies shifts from southern spring to southern winter, indicating that the physical carbon pump is becoming more dominant. Also in the following years, the Southern Ocean acts as a source of CO<sub>2</sub> to the atmosphere. Initially, the strongest positive anomalies of the CO<sub>2</sub> flux are apparent at the time of the respective spring blooms in the Southern and Northern Hemisphere, indicating weaker than unperturbed blooms or a delayed bloom, as CO<sub>2</sub>-flux anomalies become negative in December of year 2–3.

To investigate the driving mechanisms of the oceanic carbon cycle anomalies further we show time series of CO<sub>2</sub>-flux (Fig. 10) and export production (Fig. 11) anomalies for the first 6 yr of each simulation as global sum for all ensemble members and the ensemble mean (Figs. 10a and 11a) and for distinct oceanic regions as ensemble mean only (Figs. 10b, c and 11b, c). The globally integrated ocean–atmosphere CO<sub>2</sub> flux anomaly (Fig. 10a) is directed into the ocean beginning at the end of year 1. At the beginning of year 2 the flux is about 0.1 GtC per month. This value increases to about 0.2 GtC per month for the ensemble mean over years 2 and 3. This is much larger than the 2 $\sigma$  interval from the control run (about 0.05 GtC per month). Superimposed on this are positive spikes in Southern Hemisphere spring (October/November of year 2 and 3), and negative spikes in December/January of year 2 and 3. This implies a dominating effect from the marine biology, consistent with a delayed Southern Ocean spring bloom, as already derived from the CO<sub>2</sub> flux maps.

Splitting the CO<sub>2</sub>-flux into different regions makes this even more clear (Fig. 10c). In particular in the Southern Ocean, the positive/negative sequence shows up for some years, but also for the individual ocean basins between 14° S and 50° S. The same delay of the spring bloom is apparent in the Northern Hemisphere, but with a phase

**BGD**

9, 8693–8732, 2012

## Impact of supervolcanic eruptions on the Earth System

J. Segschneider et al.

Title Page

Abstract

Introduction

Conclusions

References

Tables

Figures

⏪

⏩

◀

▶

Back

Close

Full Screen / Esc

Printer-friendly Version

Interactive Discussion

shift of six months and less pronounced. This is also demonstrated by time series of the export production (Fig. 11). The global integral shows anomalously low export production in October/November, and relatively high values in December (Fig. 11a). Both extremes leave the  $\pm 2\sigma$  interval. Looking into different regions (Fig. 11b, c) again reveals that the largest signals come from the Southern Ocean (Fig. 11c). Interestingly, while the negative anomalies disappear after year 3, the positive anomalies prevail for another 3 yr, albeit weakening.

The tropical ocean reacts differently and the time series vary more smoothly, both for CO<sub>2</sub>-flux (Fig. 10b) and export production (Fig. 11b). Whereas the CO<sub>2</sub>-flux anomaly in the tropical Pacific returns to zero 3 yr after the eruption, the export production shows positive anomalies from 2 yr after the eruption until 5 yr after the eruption. The amplitude of this positive anomaly is even slightly larger than the initial negative anomalies.

### 3.2.3 Terrestrial carbon cycle response

In this section we investigate the terrestrial carbon cycle further by analyzing the spatial distribution of anomalies of the vegetation and soil carbon pools. Maps of carbon storage anomalies for the ensemble mean are shown in Fig. 12 as annual means for year 2, 5, 50, and 200 of the model integration.

For the vegetation (Fig. 12a–d) anomalies with a distinct pattern – negative anomalies in regions of temperate climate, and positive anomalies in tropical regions, in particular the tropical rain forests of the Amazon and Central Africa – are present already in year 2 (Fig. 12a). This pattern in principle persists until the end of the experiment (Fig. 12d) in year 200. This is in so far interesting as the global mean vegetation pool anomaly is close to zero already in year 5 (Fig. 8). The maps demonstrate that locally, perturbations of the vegetation carbon pool persist for much longer. Locally, perturbations are largest around year 5 (Fig. 12b) and are only slightly less in year 50 (Fig. 12c). In year 200 (Fig. 12d) the anomaly pattern is still similar to that of year 5 but the anomalies are less than half the maximum values in most regions. Note that, due to too wet conditions in the atmospheric model compartment for the desert regions of Australia,

## Impact of supervolcanic eruptions on the Earth System

J. Segschneider et al.

[Title Page](#)[Abstract](#)[Introduction](#)[Conclusions](#)[References](#)[Tables](#)[Figures](#)[Back](#)[Close](#)[Full Screen / Esc](#)[Printer-friendly Version](#)[Interactive Discussion](#)

JSBACH tends to simulate higher than observed vegetation cover in Central Australia and thus most likely too large a response of the Australian vegetation carbon pool to the volcanic forcing. Note also that, since this model study is based on pre-industrial conditions, the extent of the tropical rainforests is larger in the model than for present day (as is the case, e.g., on the east coast of Australia).

For the soil pool (Fig. 12e–h), we find a similar anomaly pattern as for the vegetation, with a carbon gain in the tropical regions and carbon loss in the higher latitudes after the volcanic eruption already from year 2 (Fig. 12f). In the higher latitudes this response is driven by reduced litter input from the slower growing vegetation, whereas in the tropical regions the reduced respiration in response to the cooling dominates the carbon content anomalies. In year 5, maximum anomalies are up to  $-500 \text{ molC m}^{-2}$  e.g., in the Amazon region. The anomaly pattern persists even stronger than for the vegetation (Fig. 12g, h) and anomalies only slowly become smaller.

From the global anomalies time series of soil carbon content (Fig. 8) it is evident that the reduced respiration in the tropical regions dominates the global long term land carbon cycle response. Any additional carbon in the soil pool in response to the volcano induced cooling is respired with the set time scale of respiration in the soil (100 yr) once temperatures are back to normal. It is, therefore, more expected for the soil pool than for the vegetation that the anomaly pattern persists for much longer than the temperature perturbation (Fig. 2).

## 4 Discussion

We will first address the question why the land compartment reacts more sensitively to the volcano induced climate perturbation than the ocean (see section 3.2.1 and Fig. 8). A central point here is to understand how the ocean and land differ in their response to a change in the carbon content of the respective other compartment: the dynamical link between the oceanic and terrestrial carbon pools is the atmosphere. Any change in the carbon content of the land or ocean pool will change the atmospheric carbon

**BGD**

9, 8693–8732, 2012

### Impact of supervolcanic eruptions on the Earth System

J. Segschneider et al.

Title Page

Abstract

Introduction

Conclusions

References

Tables

Figures

⏪

⏩

◀

▶

Back

Close

Full Screen / Esc

Printer-friendly Version

Interactive Discussion



content. But, while the flux between ocean and atmosphere depends strongly on the difference in partial pressure between atmosphere and surface ocean, the flux between land compartment and atmosphere does not directly depend on the partial pressure of the atmosphere.

5 This holds for the system as considered here even though a weak impact of the ocean on the land could come from reduced CO<sub>2</sub>-fertilization of the land biosphere as the ocean initially takes up CO<sub>2</sub>. But for the relatively small and short  $p\text{CO}_2$  changes induced by the oceanic uptake, these effects are only small: from the initial oceanic uptake of 6 GtC the atmospheric  $p\text{CO}_2$  would decrease by 3 ppm. Norby et al. (2005),  
10 for various types of forest estimate a net primary productivity (NPP) increase of 23 % for a doubling of atmospheric CO<sub>2</sub> from 280 ppm to 560 ppm. Assuming a NPP of 60 GtC, the impact would be a reduction of NPP by 0.15 GtC.

The cause-effect sequence after the volcanic eruption then is as follows: after an initial loss of vegetation, both the ocean and the land tend to take up more carbon  
15 as a result of the volcano induced cooling. The gain of carbon in the land carbon pool as simulated by the model decreases the atmospheric  $p\text{CO}_2$ , causing a negative atmosphere-ocean partial pressure difference anomaly. This drives an immediate flux from the ocean to the atmosphere. As a result, the inherent oceanic behaviour as a sink of atmospheric carbon is overruled by the land compartment's gain and the ocean is  
20 turned into a source of carbon for the atmosphere five years after the eruption. The atmosphere has no carbon dynamics on its own and in this sense it merely is a passive reservoir that reacts to the fluxes from the land and the ocean. It should be kept in mind, however, that the dynamics of the atmosphere, in particular surface temperature, winds and precipitation, are the major drivers of the land and ocean carbon reservoirs.

25 A second question is why the strong cooling does not result in a more substantial uptake of CO<sub>2</sub> by the ocean via the solubility pump. Broecker and Peng (1982) estimate a decrease of 10 ppm in ocean partial pressure for a cooling by 1 K on decadal time scales. For our maximum cooling by 4 K, this would mean a 40 ppm decrease in ocean  $p\text{CO}_2$ . This indicates that there is a potential for the solubility pump to play a strong

**BGD**

9, 8693–8732, 2012

---

## Impact of supervolcanic eruptions on the Earth System

J. Segschneider et al.

---

Title Page

Abstract

Introduction

Conclusions

References

Tables

Figures

⏪

⏩

◀

▶

Back

Close

Full Screen / Esc

Printer-friendly Version

Interactive Discussion



role in response to temperature variations. We will now try to understand why the simulated oceanic uptake is weaker than could be inferred from the above estimate of the sensitivity of the solubility pump. First, the volcano induced cooling over the ocean is only half (3 K) of what it is over land (6 K), and it lasts only for a few years before becoming substantially weaker (Fig. 3). Both the relatively weak oceanic cooling and the time scale of the perturbation thus limit the oceanic response. In our experiments, the physical pump is additionally counteracted by a decrease in export production at the time of maximum perturbation (2–3 yr after the eruption, Sect. 3.2.2, Fig. 11). In the Southern Ocean anomalous carbon fluxes (Fig. 5e–h) are likely driven by changing zonal winds (Fig. 5a–d) and in the equatorial belt also by changed upwelling patterns (Fig. 6) but it is not possible to disentangle and quantify these effects with the current model set-up.

Next, we discuss the additional information that we gain from performing an ensemble simulation as compared to a single realisation. The spread of the ensemble for the maximum temperature anomaly (1 K) relates to about 25 % of the simulated temperature response (–3.3 K to –4.3 K, Fig. 2). The coldest ensemble members in year 3 (anomaly of more than –4 K) are initialized from a moderate La Niña, and one moderate and one strong El Niño. In year 4, the coldest member is initialized from a strong La Niña, and the cooling is also stronger than –4 K, indicating that not only the amplitude but also the timing of the maximum cooling can vary considerably amongst ensemble members. Deviations of the neutral ENSO initialized runs from the ensemble mean temperature anomaly are often as large as for other initializations, but neutral ENSO runs seldom form the boundaries of the ensemble. In summary this indicates that one could misinterpret the amplitude of the maximum cooling by up to 25 % and the timing by one year when performing only a single realization of the volcanic perturbation. Moreover, it cannot be argued that starting from neutral ENSO conditions would result in an experiment similar to the ensemble mean.

This holds even more for the atmospheric  $p\text{CO}_2$ , where the spread of the perturbation is even larger compared to the maximum anomaly (4 ppm compared to a signal of

## BGD

9, 8693–8732, 2012

### Impact of supervolcanic eruptions on the Earth System

J. Segschneider et al.

Title Page

Abstract

Introduction

Conclusions

References

Tables

Figures



Back

Close

Full Screen / Esc

Printer-friendly Version

Interactive Discussion



3–7 ppm and an ensemble mean anomaly of about 5 ppm, Fig. 9). This also demonstrates the need for ensemble simulations that sample the climate system state at the time of eruption when investigating the response of the Earth System to volcanic eruptions.

5 In comparison with the simulation of the 1258 AD volcanic eruption (Brovkin et al., 2010), the results for the Yellowstone-like eruption differ in addition to the larger amplitude in the climatic and carbon cycle signals also qualitatively. They show a different response of the marine and terrestrial ecosystems. While the marine ecosystem was largely unaffected by the smaller scale eruption, the stronger eruption leads to a reduction of the marine export production and a retardation of the spring plankton bloom on both hemispheres in the 2 yr after the eruption. This shift of the bloom may have an impact on higher trophic levels as the supply of edible biomass will also shift in time. The stronger eruption also triggers a negative anomaly of the terrestrial vegetation in the first 2–3 yr (Fig. 8) after the eruption which is not present for the 1258 AD eruption. 10 Our 200 yr long experiment reveals that locally, perturbations of the terrestrial carbon pools persist for much longer than the climate perturbation.

The location and season of the eruption may also have an impact on the response of the climate system. We also analysed a smaller ensemble of a Yellowstone-like winter eruption, and YTT summer and winter eruptions. This analysis indicates that with regard to the very large eruption investigated here the impact of the latitude of the eruption (Northern Hemisphere vs. tropics) on the carbon cycle is only small (about 0.5 ppm for the maximum perturbation of atmospheric  $p\text{CO}_2$  between ensemble means, figure not shown). Also the season of the eruption (summer vs. winter) has a similarly small impact. Overall, the deviations from varying location and season of the volcanic eruption are smaller than the spread of the ENSO-based ensemble analysed here (4 ppm). 20 25

When comparing our results to the study of Frölicher et al. (2011), we find that the sensitivity of the carbon cycle of the MPI-ESM is lower than that of the NCAR CSM1.4-carbon. The MPI-ESM response of atmospheric  $p\text{CO}_2$  to a cooling of 3.3 K–4.3 K is a decrease by 4–7 ppm, while for the NCAR CSM4.1 for a cooling of 2.2 K it is about

## Impact of supervolcanic eruptions on the Earth System

J. Segschneider et al.

[Title Page](#)[Abstract](#)[Introduction](#)[Conclusions](#)[References](#)[Tables](#)[Figures](#)[Back](#)[Close](#)[Full Screen / Esc](#)[Printer-friendly Version](#)[Interactive Discussion](#)

8 ppm and for a cooling of 4 K it is close to 12 ppm (10 × Pinatubo case, Frölicher et al., 2011). This may be due to the temporal evolution of the land vegetation: while in the MPI-ESM, there is an initial decrease of the vegetation pool of 4 GtC at the time of maximum ocean uptake (thereby limiting the atmospheric  $p\text{CO}_2$  anomaly), in the NCAR CSM1.4-carbon such a temporal behaviour only occurs for the 100 × Pinatubo case (with a maximum cooling of 8 K compared to 3.3 K–4.3 K for our 100 × Pinatubo cases).

Climate-carbon cycle feedbacks can be neglected even for supervolcanic eruptions: the ensemble mean atmospheric  $\text{CO}_2$  decrease by about 6 ppm needs to be put in relation to a transient climate sensitivity of 2.2 K for a doubling of  $\text{CO}_2$  for the MPI-ESM. (Note that the transient climate sensitivity is much weaker than the equilibrium climate sensitivity, which is 3.4 K for the MPI-ESM). For the MPI-ESM a change of 6 ppm in atmospheric  $\text{CO}_2$  would lead to a temperature change of only about 0.02 K. Even assuming that the perturbation lasts long enough for the equilibrium climate sensitivity of the model (3.4 K) to be relevant, the feedback-caused temperature decrease would only be around 0.03 K, which is negligible compared to the simulated range of temperature decrease (3.3 K–4.3 K) and even the variations arising from different initial conditions (1 K). We thus contradict the statement of Frölicher et al. (2011) that their “multidecadal” decrease in atmospheric  $\text{CO}_2$  leads to a significant cooling and perturbs the Earth System on time scales much longer than the residence time of the volcanic aerosols due to climate-carbon cycle feedbacks – the perturbations are simply too small to be relevant in this regard.

Even though we employ a comprehensive ESM, our study has some limitations. First, we do not take into account tephra on land with its potential impact on vegetation and albedo, on land and sea ice. The large caldera forming eruptions at Yellowstone have spread volcanic ash over large parts of the North American continents covering 1/3 of the US with a tephra layer (e.g., Perkins and Nash, 2002; Sparks et al., 2005; Jones et al., 2007). In sensitivity experiments we investigated the impact of tephra on the carbon cycle for a Yellowstone summer eruption including tephra and found

**BGD**

9, 8693–8732, 2012

## Impact of supervolcanic eruptions on the Earth System

J. Segschneider et al.

Title Page

Abstract

Introduction

Conclusions

References

Tables

Figures

⏪

⏩

◀

▶

Back

Close

Full Screen / Esc

Printer-friendly Version

Interactive Discussion

no significant global impact. This agrees with the simulation by Jones et al. (2005), who could show that the ash blanket from Yellowstone has a significant impact on atmospheric circulation but not on the global climate.

It has also been discussed that the input of iron and other nutrients from the coatings of volcanic ashes to the ocean has a potential for fertilization of the marine biology (e.g., Duggen et al., 2007) and that this could explain the observed dip in atmospheric CO<sub>2</sub> concentration rise after the 1991 Mt. Pinatubo eruption (Watson, 1997). In the latter study, however, iron input to the ocean was assumed to originate from sulfate aerosols, that have a lifetime of several years and are spread globally, while the leaching experiments of Duggen et al. (2007) were performed on volcanic ash, which is different from the sulfate aerosols. The fine ash is deposited within weeks and relatively close to the source region (Niemeier et al., 2009). To test if the input of fine ash to the ocean has an impact on the marine carbon cycle, we simulated the impact of iron fertilization from the Mt. Pinatubo and Cerro Hudson eruption in 1991, using simulated fine ash deposition fields from Niemeier et al. (2009) and release rates of iron and nutrients from Jones and Gislason (2008) in an ocean only setup of MPIOM/HAMOCC. Also in this experiment we did not find a significant impact on the marine carbon cycle. This might be different for large volcanic eruptions that deposit larger amounts of iron to the Southern Ocean, the largest iron limited region in the world ocean. Release of poisonous substances from the ash coatings might, on the other hand, limit the biological production.

Limitations of the employed terrestrial vegetation model are that it does not take into account higher photosynthesis rates due to more diffusive radiation that may occur after volcanic eruptions (Gu et al., 2003). Using evidence from tree rings, however, Krakauer and Randerson (2003) did not find enhanced primary production following volcanic eruptions, implying that the neglect of diffuse radiation impact on plant growth does not severely limit our study. Productivity limitation by nutrients (i.e., nitrogen) and a dynamic vegetation are not yet included in the land model version used here.

## Impact of supervolcanic eruptions on the Earth System

J. Segschneider et al.

Title Page

Abstract

Introduction

Conclusions

References

Tables

Figures



Back

Close

Full Screen / Esc

Printer-friendly Version

Interactive Discussion



## 5 Conclusions

In this study we investigated the simulated response of climate and the carbon cycle to a Yellowstone-like super volcanic eruption with a fully comprehensive ESM. In response to AOD perturbations representing a Yellowstone volcanic super eruption, the simulated global mean surface temperature dropped by between 3.3K–4.3K for different ensemble members. The response is strongly asymmetric, with much stronger cooling over the Northern Hemisphere land surface (up to  $-10$  K) than over the Southern Hemisphere sea surface (less than  $-2$  K over large regions of the Southern Ocean). Consequently, the terrestrial carbon cycle experiences a stronger perturbation than the marine carbon cycle. The terrestrial carbon cycle initially responds with a drop in vegetation storage in response to the decrease in radiation. After 2 yr this is overruled by an increase of carbon in the soil pool due to decreasing temperature and hence reduced respiration of organic matter in the soil. For the marine carbon cycle, we analyse an increase in solubility and a decrease of biological production in the first few years. An interesting feature here is, that not only the biological export production decreases for some years, but also that there is a delay of the planktonic spring bloom in mid-to-high latitudes on both hemispheres, with possible impacts on higher trophic levels. After a few years, the ocean turns into a carbon source for the atmosphere as atmospheric  $p\text{CO}_2$  decreases in response to the land's soil pool gain. The long term response of the system is a weak flow from the ocean to the atmosphere, set by the time scale of respiration in the land slow soil pool. At the end of the integration, 200 yr after the eruption, both components did not return to pre-eruption levels.

The response of the carbon cycle to the volcanic eruption can be described by 4 phases: in the first year, the land biosphere pool is decreased in response to the reduced short wave radiation. During year 2–3 the ocean and soil take up carbon in response to the cooling. From year 4–20, the soil carbon pool increases due to still negative temperature anomalies, and the ocean releases carbon to compensate for reduced atmospheric  $p\text{CO}_2$  caused by the soil carbon pool increase. After year 20, the

**BGD**

9, 8693–8732, 2012

### Impact of supervolcanic eruptions on the Earth System

J. Segschneider et al.

Title Page

Abstract

Introduction

Conclusions

References

Tables

Figures

⏪

⏩

◀

▶

Back

Close

Full Screen / Esc

Printer-friendly Version

Interactive Discussion

soil carbon pool slowly releases the additional carbon after temperatures returned to pre-eruption levels, and the ocean slowly gains back the previously released carbon. The equilibrium state after 200 yr is slightly different from before the eruption.

Moreover, the response of the coupled system is different from the sum of the responses of the individual components, emphasizing the need to employ coupled climate-carbon cycle models to estimate the impact of volcanic eruptions on the dynamics of the carbon cycle.

*Acknowledgements.* This work benefits from stimulating discussions within the MPIM Super Volcano and Millennium projects. J. S. acknowledges funding from the CliSAP excellence cluster at the KlimaCampus Hamburg, C. T. financial support by the German Science Foundation (DFG, Collaborative Research Centre 574). Computations were carried out at the German Climate Computing Centre (DKRZ).

The service charges for this open access publication have been covered by the Max Planck Society.

## References

- Ambrose, S. H.: Late Pleistocene human population bottlenecks, volcanic winter, and differentiation of modern humans, *J. Hum. Evol.*, 34, 623–651, 1998. 8695
- Ammann, C., Meehl, G., Washington, W., and Zender, C.: A monthly and latitudinally varying volcanic forcing dataset in simulations of 20th century climate, *Geophys. Res. Lett.*, 30, 1657–1671, doi:10.1029/2003GL016875, 2003. 8697
- Broecker, W. S. and Peng, T. H. (eds.): *Tracers in the Sea*, Lamont-Doherty Geological Observatory, Columbia University, NY, 1982. 8710
- Brovkin, V., Lorenz, S., Jungclauss, J., Raddatz, T., Timmreck, C., Reick, C., Segschneider, J., and Six, K.: Sensitivity of a coupled climate-carbon cycle model to large volcanic eruptions during the last millennium, *Tellus B*, 62B, 674–681, 2010. 8696, 8697, 8698, 8702, 8712
- Duggen, S., Croot, P., Schacht, U., and Hoffmann, L.: Subduction zone volcanic ash can fertilize the surface ocean and stimulate plankton growth: evidence from biogeochemical ex-

**BGD**

9, 8693–8732, 2012

## Impact of supervolcanic eruptions on the Earth System

J. Segschneider et al.

Title Page

Abstract

Introduction

Conclusions

References

Tables

Figures



Back

Close

Full Screen / Esc

Printer-friendly Version

Interactive Discussion



## Impact of supervolcanic eruptions on the Earth System

J. Segsneider et al.

Title Page

Abstract

Introduction

Conclusions

References

Tables

Figures

⏪

⏩

◀

▶

Back

Close

Full Screen / Esc

Printer-friendly Version

Interactive Discussion

periments and satellite data, *Geophys. Res. Lett.*, **34**, LO1612, doi:10.1029/2006GL027522, 2007. 8714

Frölicher, T. L., Joos, F., and Raible, C. C.: Sensitivity of atmospheric CO<sub>2</sub> and climate to explosive volcanic eruptions, *Biogeosciences*, **8**, 2317–2339, doi:10.5194/bg-8-2317-2011, 2011. 8697, 8712, 8713

Gu, L., Baldocchi, D., Wofsy, S., Munger, J., Michalsky, J., Urbanski, S., and Boden, T.: Response of a deciduous forest to the Mount Pinatubo eruption: enhanced photosynthesis, *Science*, **299**, 2035–2038, 2003. 8714

Jones, C. and Cox, P.: Modelling the volcanic signal in the atmospheric CO<sub>2</sub> record, *Global Biogeochem. Cy.*, **15**, 453–465, 2001. 8696, 8697

Jones, G., Gregory, J., Stott, P., Tett, S., and Thorpe, R.: An AOGCM simulation of the climate response to a volcanic super-eruption, *Clim. Dynam.*, **25**, 725–773, 2005. 8695, 8714

Jones, M. and Gislason, S.: Rapid release of metal salts and nutrients following the deposition of volcanic ash into aqueous environments, *Geochim. Cosmochim. Ac.*, **72**, 3661–3680, 2008. 8714

Jones, M., Sparks, R., and Valdes, P.: The climatic impact of supervolcanic ash blankets., *Clim. Dynam.*, **29**, 553–564, doi:10.1007/s00382-007-0248-7, 2007. 8713

Jungclaus, J. H., Lorenz, S. J., Timmreck, C., Reick, C. H., Brovkin, V., Six, K., Segsneider, J., Giorgetta, M. A., Crowley, T. J., Pongratz, J., Krivova, N. A., Vieira, L. E., Solanki, S. K., Klocke, D., Botzet, M., Esch, M., Gayler, V., Haak, H., Raddatz, T. J., Roeckner, E., Schnur, R., Widmann, H., Claussen, M., Stevens, B., and Marotzke, J.: Climate and carbon-cycle variability over the last millennium, *Clim. Past*, **6**, 723–737, doi:10.5194/cp-6-723-2010, 2010. 8696, 8698

Krakauer, N. and Randerson, J.: Do volcanic eruptions enhance or diminish net primary production? Evidence from tree rings, *Global Biogeochem. Cy.*, **17**, 1118, doi:10.1029/2003GB002076, 2003. 8714

Maier-Reimer, E.: Geochemical cycles in an ocean general circulation model: preindustrial tracer distributions, *Global Biogeochem. Cy.*, **7**, 645–677, 1993. 8698, 8699

Maier-Reimer, E., Kriest, I., Segsneider, J., and Wetzol, P.: The HAMburg Ocean Carbon Cycle model HAMOCC5.1 – Technical description Release 1.1, Reports on Earth System Science 14, Max Planck Institute for Meteorology, 2005. 8698

## Impact of supervolcanic eruptions on the Earth System

J. Segschneider et al.

Title Page

Abstract

Introduction

Conclusions

References

Tables

Figures

⏪

⏩

◀

▶

Back

Close

Full Screen / Esc

Printer-friendly Version

Interactive Discussion



- Marsland, S. J., Haak, H., Jungclaus, J., Latif, M., and Röske, F.: The Max Planck Institute global ocean/sea ice model with orthogonal curvilinear coordinates, *Ocean Modell.*, 5, 91–127, 2003. 8698
- Nemani, R., Keeling, C., Hashimoto, H., Jolly, W., Piper, S., Tucker, C., Myneni, R., and Running, S.: Climate-driven increases in global terrestrial net primary production from 1982 to 1999, *Science*, 300, 1560–1563, doi:10.1126/science.1082750, 2003. 8697
- Niemeier, U., Timmreck, C., Graf, H.-F., Kinne, S., Rast, S., and Self, S.: Initial fate of fine ash and sulfur from large volcanic eruptions, *Atmos. Chem. Phys.*, 9, 9043–9057, doi:10.5194/acp-9-9043-2009, 2009. 8700, 8714
- Norby, R., DeLucia, E., Gielen, B., Calfapietra, C., Giardina, C., King, J., Ledford, J., McCarthy, H., Moore, D., Ceulemans, R., Angelis, P. D., Finzi, A., Karnosky, D., Kubiske, M., Lukac, M., Pregitzer, K., Scarascia-Mugnozza, G., Schlesinger, W., and Oren, R.: Forest response to elevated CO<sub>2</sub> is conserved across a broad range of productivity, *P. Natl. Acad. Sci. USA*, 102, 18052–18056, 2005. 8710
- Penland, C., Sun, D.-Z., Capotondi, A., and Vimont, D. J.: A brief introduction to El Niño and La Niña, in: *Climate Dynamics: Why does Climate vary?*, *Geoph. Monog. Series*, 189, 53–64, doi:10.1029/2008GM000846, 2010. 8701
- Perkins, M. and Nash, B.: Explosive silicic volcanism of the Yellowstone hotspot: the ash fall tuff record, *Geol. Soc. Am. Bull.*, 114, 367–381, 2002. 8713
- Raddatz, T. J., Reick, C. J., Knorr, W., Kattge, J., Roeckner, E., Schnur, R., Schnitzler, K.-G., Wetzol, P., and Jungclaus, J.: Will the tropical land biosphere dominate the climate-carbon cycle feedback during the twenty-first century?, *Clim. Dynam.*, 29, 565–574, 2007. 8698
- Read, W. G., Froidevaux, L., and Waters, J. W.: Microwave limb sounder measurements of 25 stratospheric SO<sub>2</sub> from the Mt. Pinatubo volcano, *Geophys. Res. Lett.*, 20, 1299–1302, 1993. 8701
- Robock, A., Ammann, C., Oman, L., Shindell, D., Levis, S., and Stenchikov, G.: Did the Toba volcanic eruption of 74 ka B.P. produce widespread glaciation?, *J. Geophys. Res.*, 114, D10107, doi:10.1029/2008JDO11652, 2009. 8695
- Roeckner, E., Bäuml, G., Bonaventura, L., Brokopf, R., and Esch, M.: The Atmospheric General Circulation Model ECHAM5. Part I: Model Description, Report 349, Max Planck Institute for Meteorology, 2003. 8698

---

## Impact of supervolcanic eruptions on the Earth System

J. Segschneider et al.

---

Title Page

Abstract

Introduction

Conclusions

References

Tables

Figures

⏪

⏩

◀

▶

Back

Close

Full Screen / Esc

Printer-friendly Version

Interactive Discussion



- Rothenberg, D., Mahowald, N., Lindsay, K., Doney, S. C., Moore, J. K., and Thornton, P.: Volcano impacts on climate and biogeochemistry in a coupled carbon-climate model, *Earth Syst. Dynam. Discuss.*, 3, 279–323, doi:10.5194/esdd-3-279-2012, 2012. 8697
- 5 Self, S.: The effects and consequences of very large explosive volcanic eruptions, *Philos. T. R. Soc. A*, 364, 2073–2097, 2006. 8695
- Self, S. and Blake, S.: Consequences of explosive supereruptions, *Elements*, 4, 41–46, 2008. 8695
- Six, K. and Maier-Reimer, E.: Effects of plankton dynamics on seasonal carbon fluxes in a ocean general circulation model, *Global Biogeochem. Cy.*, 10, 559–583, 1996. 8699
- 10 Sparks, R., Self, S., Grattan, J., Oppenheimer, C., Pyle, D., and Rymer, H.: Supereruptions: global effects and future threats, Geological Society of London, available at: www.geolsoc.org.uk/supereruptions, 2005. 8713
- Thompson, D., Wallace, J., Jones, P., and Kennedy, J.: Identifying signatures of natural climate variability in time series of global-mean surface temperature: methodology and insights, *J. Climate*, 22, 6120–6141, 2009. 8696
- 15 Timmreck, C. and Graf, H.-F.: The initial dispersal and radiative forcing of a Northern Hemisphere mid-latitude super volcano: a model study, *Atmos. Chem. Phys.*, 6, 35–49, doi:10.5194/acp-6-35-2006, 2006. 8701
- Timmreck, C., Graf, H., Lorenz, S., Niemeier, U., Zanchettin, D., Matei, D., Jungclaus, J., and Crowley, T.: Aerosol size confines climate response to volcanic super-eruptions, *Geophys. Res. Lett.*, 37, L24705, doi:10.1029/2010GL045464, 2010. 8695, 8700, 8701
- 20 Timmreck, C., Graf, H., Zanchettin, D., Hagemann, S., Kleinen, T., and Krüger, K.: Climate response to the Toba super-eruption: regional changes, *Quaternary Int.*, 258, 30–44, 2012. 8695, 8701
- 25 Tjiputra, J. and Ottera, O.: Tjiputra, J. F. and Otterå, O. H.: Role of volcanic forcing on future global carbon cycle, *Earth Syst. Dynam.*, 2, 53–67, doi:10.5194/esd-2-53-2011, 2011. 8696
- Watson, A.: Volcanic iron, CO<sub>2</sub>, ocean productivity and climate, *Nature*, 385, 587–588, 1997. 8714
- Wicks, C., Thatcher, W., Dzurisin, D., and Svarc, J.: Uplift, thermal unrest and magma intrusion at Yellowstone caldera, *Nature*, 440, 72–75, doi:10.1038/nature04507, 2006. 8698
- 30 Williams, M. A. J., Ambrose, S. H., van der Kaars, S., Ruehlemann, C., Chattopadhyaya, U., Pal, J., and Chauhan, P. R.: Environmental impact of the 73 ka Toba super-eruption in South Asia, *Palaeogeogr. Palaeoclimatol.*, 284, 295–314, 2009. 8695

Winguth, A. M. E., Heimann, M., Kurz, K. D., Maier-Reimer, E., Mikolajewicz, U., and Segschneider, J.: El Niño-Southern Oscillation related fluctuations of the marine carbon cycle, *Global Biogeochem. Cy.*, 8, 39–63, 1994. 8701

5 Zanchettin, D., Timmreck, C., Graf, H.-F., Rubino, A., Lorenz, S., Lohmann, K., Krüger, K., and Jungclaus, J.: Bi-decadal variability excited in the coupled ocean–atmosphere system by strong tropical volcanic eruptions, *Clim. Dynam.*, doi:10.1007/s00382-011-1167-1, 2011. 8699

**BGD**

9, 8693–8732, 2012

---

**Impact of  
supervolcanic  
eruptions on the  
Earth System**

J. Segschneider et al.

---

Title Page

Abstract

Introduction

Conclusions

References

Tables

Figures

◀

▶

◀

▶

Back

Close

Full Screen / Esc

Printer-friendly Version

Interactive Discussion

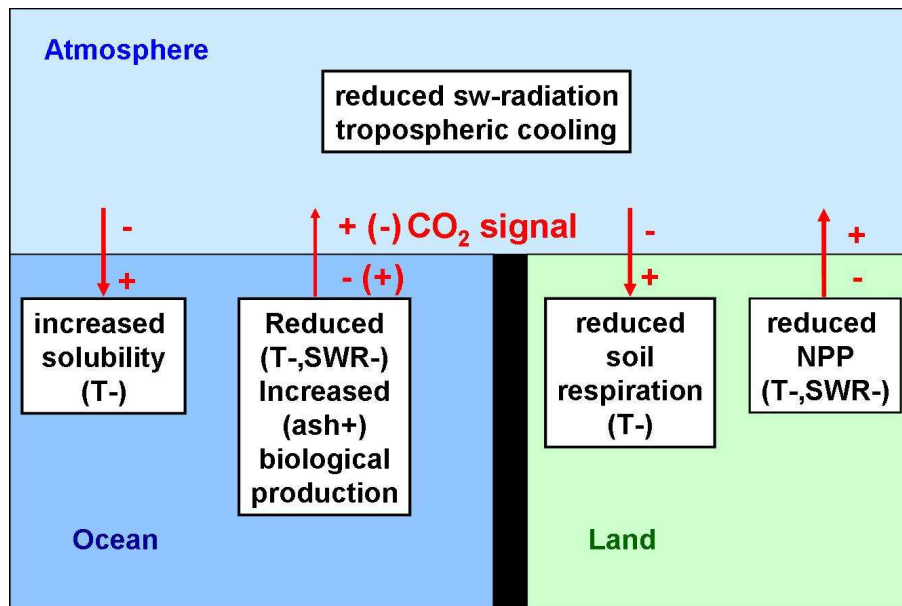


**Fig. 1.** Sketch of potential effects of volcanic eruptions on the carbon cycle. ( $T-$ ) signifies in response to negative temperature anomaly, ( $SWR-$ ) in response to negative short wave radiation anomaly, and ( $ash+$ ) in response to ash input from volcanic eruptions. Arrows indicate direction of anomalous  $CO_2$  fluxes,  $+/-$  a gain/loss of the respective reservoir,  $(-)/(+)$  in response to increased ash deposition. NPP is net primary productivity, SWR – shortwave radiation,  $T$  – temperature.

**Impact of supervolcanic eruptions on the Earth System**

J. Segschneider et al.

Title Page

Abstract Introduction

Conclusions References

Tables Figures

⏪ ⏩

◀ ▶

Back Close

Full Screen / Esc

Printer-friendly Version

Interactive Discussion



## Impact of supervolcanic eruptions on the Earth System

J. Segschneider et al.

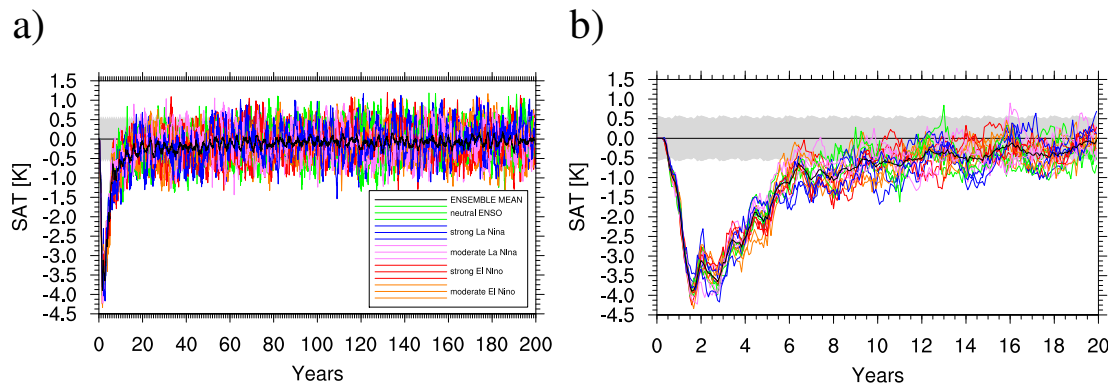


**Fig. 2.** Time series of global and monthly mean SAT anomalies (K) for **(a)** the entire 200 yr of the model experiments and **(b)** a close-up of the first 20 yr. Colours indicate the ENSO state of the control run at which the individual ensemble members were started: green for neutral ENSO, dark blue for strong La Niña, pink for moderate La Niña, red for strong El Niño and orange for moderate El Niño. The grey shaded areas indicate the monthly mean  $2\sigma$ -bar from the control experiment.

Title Page

Abstract

Introduction

Conclusions

References

Tables

Figures

◀

▶

◀

▶

Back

Close

Full Screen / Esc

Printer-friendly Version

Interactive Discussion

## Impact of supervolcanic eruptions on the Earth System

J. Segschneider et al.

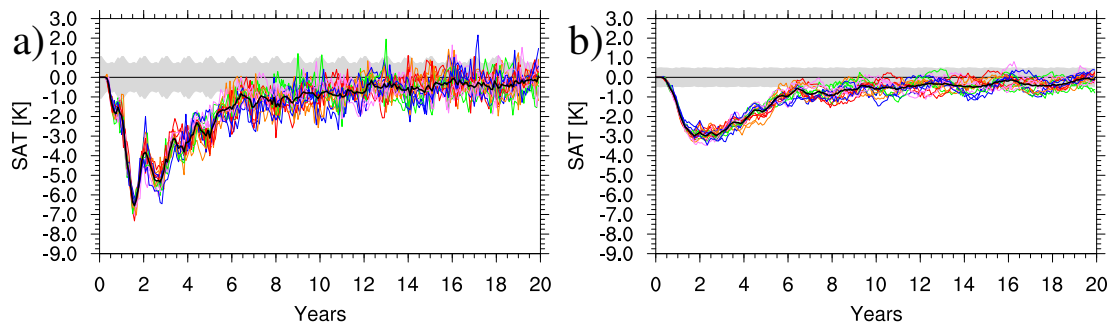


**Fig. 3.** Time series of global and monthly mean SAT anomalies over **(a)** land points only and **(b)** ocean points only for the first 20 yr of the model integrations. The grey-shaded area represents the monthly mean  $2\sigma$ -bar from the control experiment. Colours indicate the initial conditions of the integrations as in Fig. 2.

[Title Page](#)[Abstract](#)[Introduction](#)[Conclusions](#)[References](#)[Tables](#)[Figures](#)[⏪](#)[⏩](#)[◀](#)[▶](#)[Back](#)[Close](#)[Full Screen / Esc](#)[Printer-friendly Version](#)[Interactive Discussion](#)

## Impact of supervolcanic eruptions on the Earth System

J. Segschneider et al.

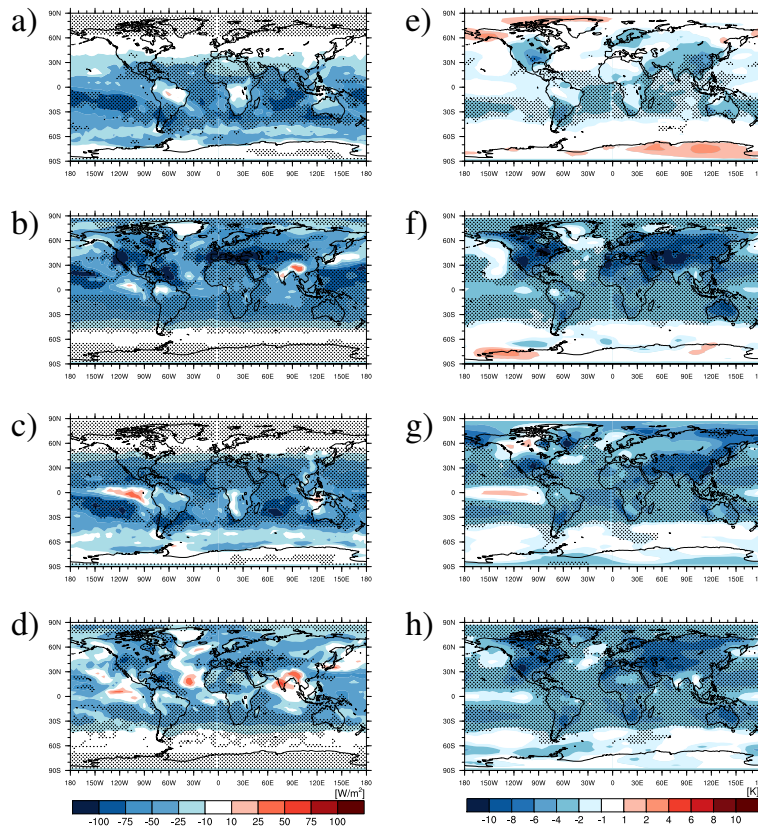


**Fig. 4.** Maps of ensemble and monthly mean anomalies of **(a–d)** short wave radiation at the Earth's surface ( $\text{Wm}^{-2}$ , left column) and **(e–h)** surface air temperature SAT (K, right column). For **(a, e)** month 12 (December year 1), **(b, f)** month 18 (June year 2), **(c, g)** month 24 (December year 2), and **(d, h)** month 30 of the experiment (June year 3). Stippled areas indicate significance of anomalies based on the  $2\text{-}\sigma$  criterion.

[Title Page](#)
[Abstract](#)
[Introduction](#)
[Conclusions](#)
[References](#)
[Tables](#)
[Figures](#)
[◀](#)
[▶](#)
[◀](#)
[▶](#)
[Back](#)
[Close](#)
[Full Screen / Esc](#)
[Printer-friendly Version](#)
[Interactive Discussion](#)

## Impact of supervolcanic eruptions on the Earth System

J. Segschneider et al.

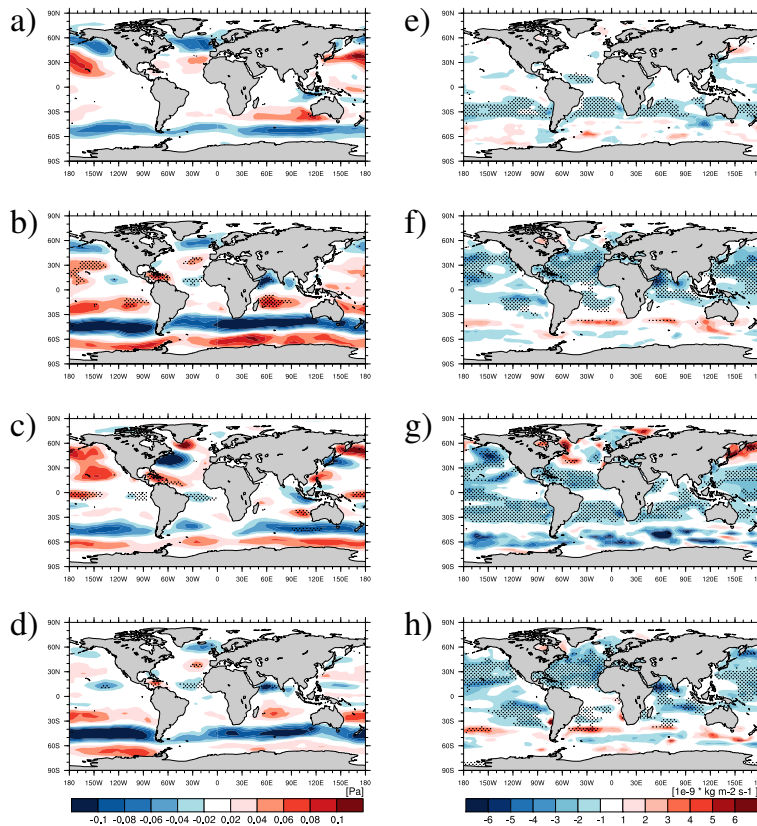


**Fig. 5.** As Fig. 4, but for (a–d) zonal wind stress  $\tau_x$  (Pa) and (e–f)  $\text{CO}_2$  flux ( $10^{-9} \text{kg C m}^{-2} \text{s}^{-1}$ ) for (a, e) month 12 (December year 1), (b, f) month 18 (June year 2), (c, g) month 24 (December year 2), and (d, h) month 30 of the experiment (June year 3). Positive anomalies of the  $\text{CO}_2$  flux indicate an anomalous flux from the ocean to the atmosphere.

Impact of  
supervolcanic  
eruptions on the  
Earth System

J. Segschneider et al.

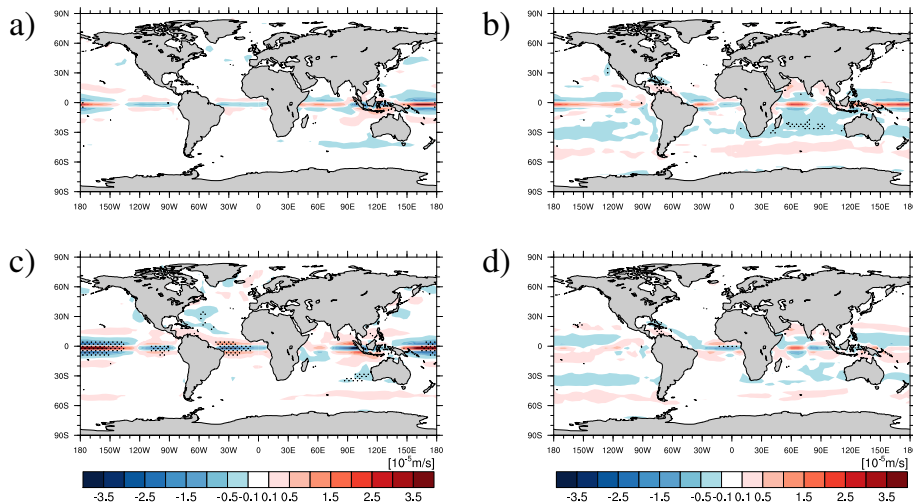


**Fig. 6.** As Fig. 4, but for Ekman pumping ( $10^{-6} \text{ m s}^{-1}$ ), for month 12 (a), 18 (b), 24 (c), and 30 (d) of the model integration. Positive anomalies indicate an anomalous upward flow.

Title Page

Abstract

Introduction

Conclusions

References

Tables

Figures



Back

Close

Full Screen / Esc

Printer-friendly Version

Interactive Discussion



## Impact of supervolcanic eruptions on the Earth System

J. Segschneider et al.

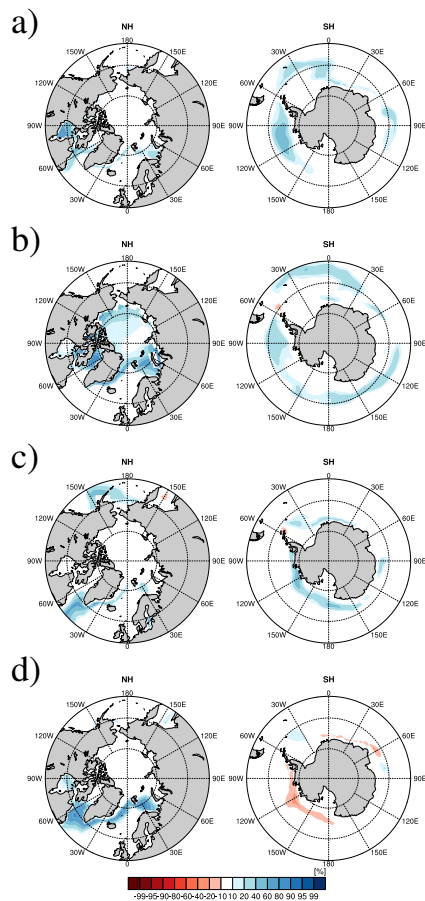


**Fig. 7.** Maps of ensemble mean anomalies of sea ice fraction (%) for month 18, 21, 27, and 72 of the model integration.

Title Page

Abstract

Introduction

Conclusions

References

Tables

Figures

⏪

⏩

◀

▶

Back

Close

Full Screen / Esc

Printer-friendly Version

Interactive Discussion

## Impact of supervolcanic eruptions on the Earth System

J. Segschneider et al.

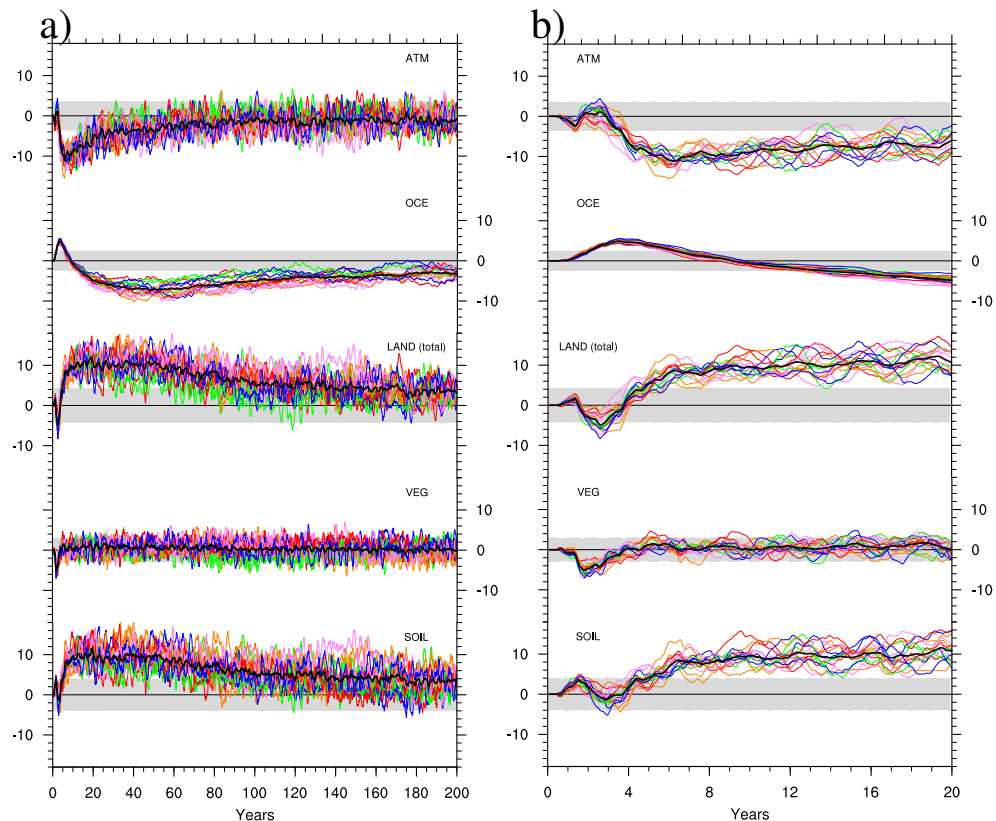


**Fig. 8.** Time series of annual mean carbon pool anomalies in GtC for (from top to bottom) the atmosphere (ATM), ocean (OCE), land vegetation and soil (LAND), and land vegetation (VEG) and land soil (SOIL) separately. The left column **(a)** shows the entire 200 yr of the experiments, the right column **(b)** the first 20 yr. The thick black line shows the ensemble mean, colours indicate initial conditions as in Fig. 2. The grey bars indicate the  $\pm 2\sigma$ -interval from the control run (see text).

Title Page

Abstract

Introduction

Conclusions

References

Tables

Figures

◀

▶

◀

▶

Back

Close

Full Screen / Esc

Printer-friendly Version

Interactive Discussion

## Impact of supervolcanic eruptions on the Earth System

J. Segschneider et al.

Title Page

Abstract

Introduction

Conclusions

References

Tables

Figures

◀

▶

◀

▶

Back

Close

Full Screen / Esc

Printer-friendly Version

Interactive Discussion

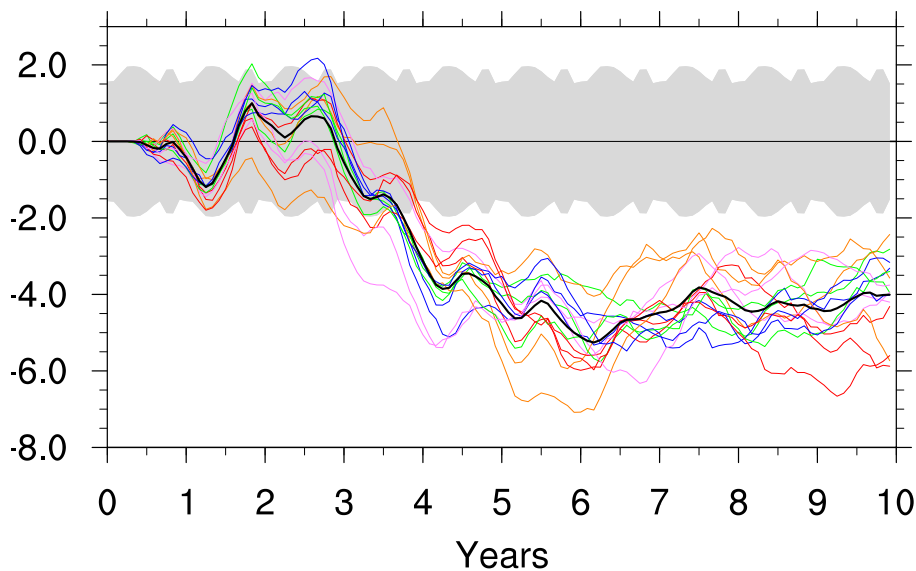


**Fig. 9.** Time series of monthly mean atmospheric  $p\text{CO}_2$  anomaly in ppm for the first 10 yr of the experiment for the ensemble mean (black line) and individual members (colored lines and grey shaded area as in Fig. 2).

## Impact of supervolcanic eruptions on the Earth System

J. Segschneider et al.

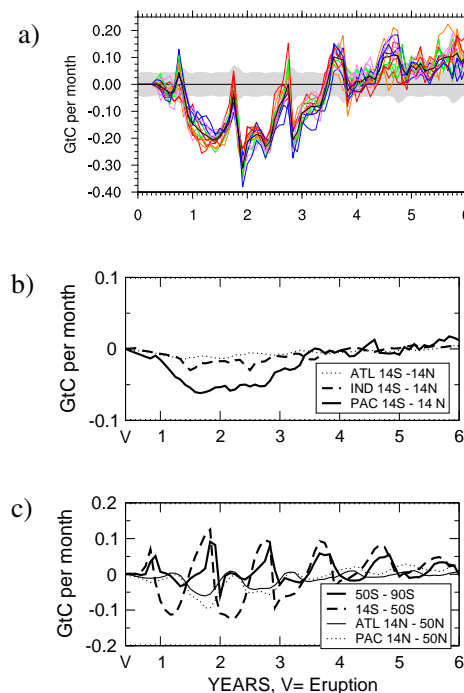


**Fig. 10.** Time series of monthly mean carbon flux anomalies between ocean and atmosphere in GtC per month for the first six years of the experiment. **(a)** globally averaged ensemble mean (black line) and individual members (colored lines and grey shaded area as in Fig. 2), **(b)** ensemble mean averaged between 14° S and 14° N in the Atlantic (dotted), the Indian Ocean (dash-dotted) and the Pacific (solid). **(c)** ensemble mean for the Southern Ocean between 50° S and 90° S (bold), for all ocean basins between 14° S and 50° S (dash-dotted), and between 14° N and 50° N for the Atlantic (thin) and the Pacific (dotted). A negative flux anomaly indicates an anomalous flux into the ocean.

[Title Page](#)
[Abstract](#)
[Introduction](#)
[Conclusions](#)
[References](#)
[Tables](#)
[Figures](#)
[Back](#)
[Close](#)
[Full Screen / Esc](#)
[Printer-friendly Version](#)
[Interactive Discussion](#)

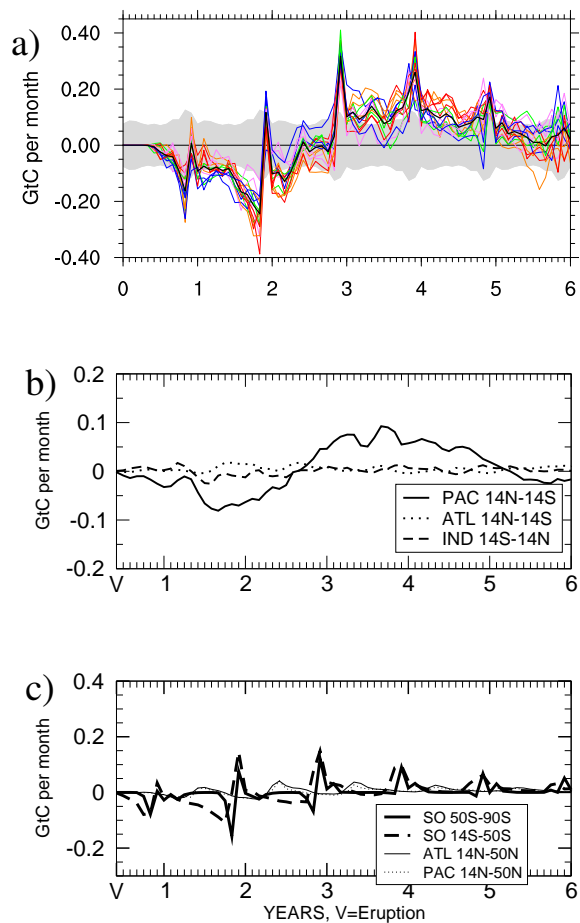


**Fig. 11.** As Fig. 10, but for the export flux of detritus at 90 m depth (the bottom of the euphotic zone in the model). Note the different scale in panel (b).

## Impact of supervolcanic eruptions on the Earth System

J. Segschneider et al.

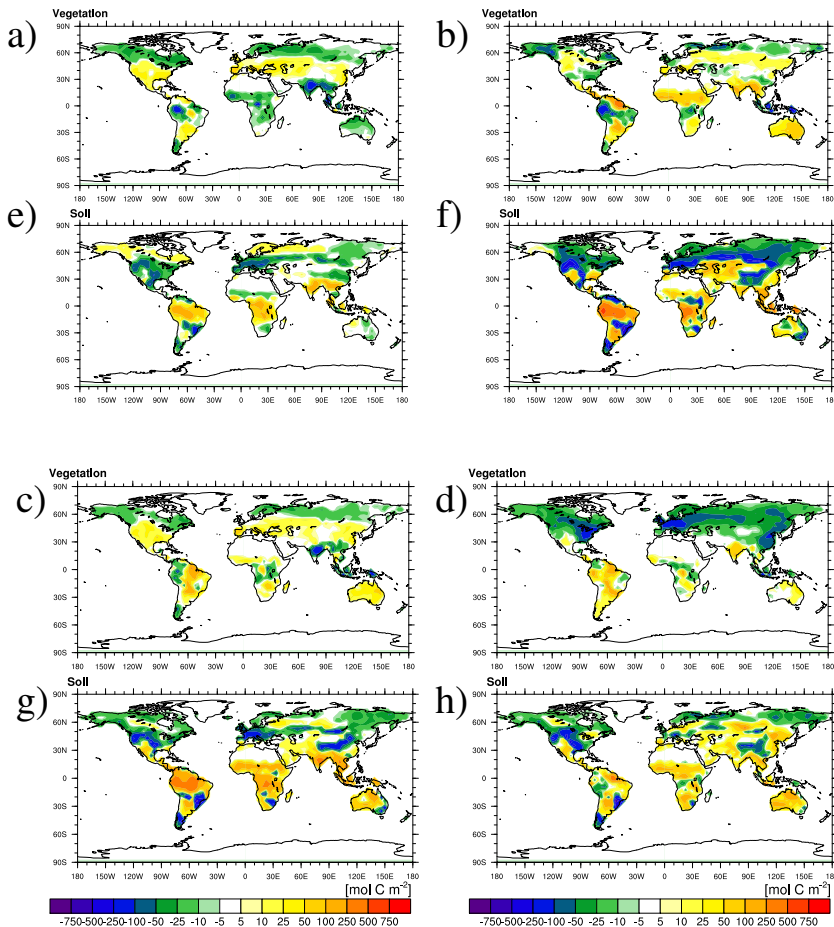


**Fig. 12.** Maps of ensemble mean land carbon pool anomalies. **(a–d)**: vegetation; **(e–f)**: soil. Annual average in ( $\text{mol C m}^{-2}$ ) for **(a, e)** year 2, **(b, f)** year 5, **(c, g)** year 50, and **(d, h)** year 200 of the experiment.

Title Page

Abstract

Introduction

Conclusions

References

Tables

Figures

⏪

⏩

◀

▶

Back

Close

Full Screen / Esc

Printer-friendly Version

Interactive Discussion